Publication Year	2022
Acceptance in OA	2025-03-08T17:58:16Z
Title	The MeerKAT Galaxy Cluster Legacy Survey: I. Survey Overview and Highlights
Authors	Knowles, K., Cotton, W. D., Rudnick, L., Camilo, F., Goedhart, S., Deane, R., RAMATSOKU, MPATI ANALICIA, Bietenholz, M. F., Brüggen, M., Button, C., Chen, H., Chibueze, J. O., Clarke, T. E., DE GASPERIN, Francesco, Ianjamasimanana, R., Józsa, G. I.G., Hilton, M., Kesebonye, K. C., Kolokythas, K., Kraan-Korteweg, R. C., Lawrie, G., Lochner, M., Loubser, S. I., Marchegiani, P., Mhlahlo, N., Moodley, K., Murphy, E., Namumba, B., Oozeer, N., Parekh, V., Pillay, D. S., Passmoor, S. S., Ramaila, A. J.T., Ranchod, S., Retana-Montenegro, E., Sebokolodi, L., Sikhosana, S. P., Smirnov, O., Thorat, K., VENTURI, Tiziana, Abbott, T. D., Adam, R. M., Adams, G., Aldera, M. A., Bauermeister, E. F., Bennett, T. G.H., Bode, W. A., Botha, D. H., Botha, A. G., Brederode, L. R.S., Buchner, S., Burger, J. P., Cheetham, T., De Villiers, D. I.L., Dikgale-Mahlakoana, M. A., Du Toit, L. J., Esterhuyse, S. W.P., Fadana, G., Fanaroff, B. L., Fataar, S., Foley, A. R., Fourie, D. J., Frank, B. S., Gamatham, R. R.G., Gatsi, T. G., Geyer, M., Gouws, M., Gumede, S. C., Heywood, I., Hlakola, M. J., Hokwana, A., Hoosen, S. W., Horn, D. M., Horrell, J. M.G., Hugo, B. V., Isaacson, A. R., Jonas, J. L., Jordaan, J. D.B., Joubert, A. F., Julie, R. P.M., Kapp, F. B., Kasper, V. A., Kenyon, J. S., Kotzé, P. P.A., Kotze, A. G., Kriek, N., Kriel, H., Krishnan, V. K., Kusel, T. W., Legodi, L. S., Lehmensiek, R., Liebenberg, D., Lord, R. T., Lunsky, B. M., Madisa, K., Magnus, L. G., Main, J. P.L., Makhaba, A., Makhathini, S., Malan, J. A.
Publisher's version (DOI)	10.1051/0004-6361/202141488
Handle	http://hdl.handle.net/20.500.12386/36550
Journal	ASTRONOMY & ASTROPHYSICS
Volume	657

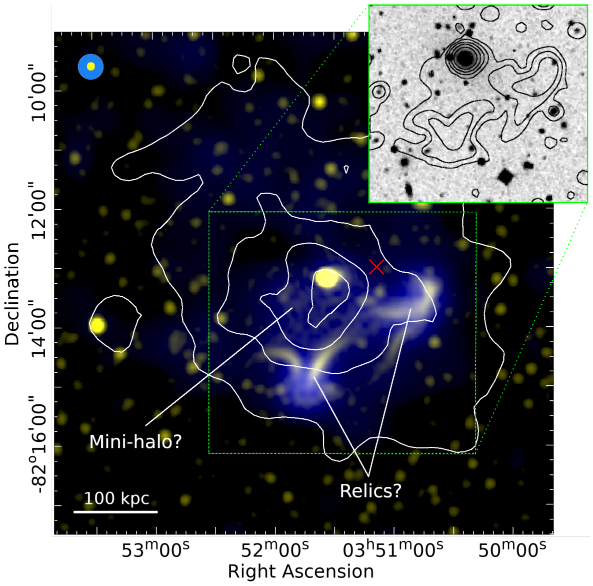

Fig. 12. MGCLS full-resolution (7.9″ × 7.5″; yellow) and filtered 25″ resolution (blue) Stokes-I intensity image of MCXC J0351.1−8212, showing newly detected candidate mini-halo and relic-like structures near the cluster centre. The corresponding synthesised beams are shown on the upper left. The colour scale is in square root scaling between 10–500 μJy beam^{-1} (yellow) and 50–800 μJy beam^{-1} (blue). Smoothed archival *Chandra* 0.5–7 keV X-ray contours (levels: 7, 12, 17, 22×10^{-8} counts cm^{-2} s^{-1}) are overlaid in white. The physical scale at the cluster redshift is indicated on the lower left, and the red × marks the NED catalogue position. Inset: DSS r-band image of the dashed region in the main figure, with 15″ resolution MGCLS contours overlaid. Contours start at 3σ = 30 μJy beam^{-1} and increase in factors of 3.

periphery of the system. We note that simulations also predict a weaker secondary shock front closer to the centre, now seen in the Coma cluster (Churazov et al. 2021). The NW candidate relic seen in MCXC J0352.4−7401 may be evidence for such a shock.

There are only a handful of double-relic clusters that also host a radio halo: for example, El Gordo (Lindner et al. 2014), CIZA J2242.8+5301 (van Weeren et al. 2010; Di Gennaro et al. 2018a), MACS J1752.0+4440 (van Weeren et al. 2012), and MACS J1149.5+2223 (Bonafede et al. 2012). Double-relic clusters are an important sub-class of merging clusters, as the merger is observed close to the plane of the sky. Systems such as MCXC J0352.4−7401 can therefore provide insights into the dynamical state of the halo emission, along with morphological and spectral properties of the transition from diffusive shock acceleration to second order turbulent re-acceleration. In addition to MCXC J0352.4−7401, there are six halo+double-relic systems in the MGCLS: known systems (El Gordo, RXC J1314−2525), and four new ones (Abell 521, MCXC J0516.6−5430, MCXC J0232.2−4420, and RXC J2351.0−1954).

6.2.2. J0351.1−8212: 'Boomerangs' and an off-centre mini-halo?

MCXC J0351.1−8212, a nearby system at z = 0.0613, is one of the newly discovered hosts of diffuse cluster emission; however, the structures seen in this system present a confusing picture. We detect a new mini-halo-like structure around, but offset from, the BCG. The source has a 1.28 GHz flux density of only 2 mJy and our preliminary estimate of the maximum linear extent in the sky plane is 240 kpc. The multi-resolution MGCLS image in Fig. 12, with white *Chandra* contours overlaid, shows the diffuse radio emission to be primarily SW of the BCG and X-ray peak, instead of being centred thereon. The size, and therefore flux density, of this possible mini-halo are difficult to clearly determine due to the presence of several brighter filamentary 'boomerang'-shaped sources less than 100 kpc from the BCG, visible in both the full-resolution (7.9″ × 7.5″) Stokes-I intensity map shown in yellow, and at 15″ resolution, indicated by black contours on the DSS r-band image of the region shown in the figure inset. The filaments do not appear to have obvious optical counterparts in DSS, and have very steep spectra ($\alpha < -2.5$) in our initial spectral maps (not shown). Going out from the X-ray peak, there is a significant decrease in the brightness from *Chandra* data at the position of the filaments. We therefore tentatively classify them as relics, although the small sizes and physical proximity to the BCG make the classification unclear.

We note the similarity of the filamentary structures to those in Abell 133 (Slee et al. 2001; Randall et al. 2010). In that case, the filaments cap a buoyant blob of AGN material from the BCG, which has dragged up cool thermal material from the cluster core. A similar process may be at work in MCXC J0351.1−8212, although why there would be two such filamentary caps is unclear. If this is another case of buoyant lifting of the radio and X-ray plasmas, then the mini-halo-like structure may in fact be the remnant of the radio lobe(s). Deeper optical imaging and investigation of the spectral shape of the various diffuse and filamentary components may be able to distinguish between the mini-halo–relic and AGN-related scenarios.

6.2.3. J0631.3−5610: Distant AGN or faint relic?

One of the strengths of MeerKAT in the L band is its extreme sensitivity to faint extended emission. Figure 13 shows an example of one of the fainter relic-like structures detected in this survey, with the left inset panel showing the full-resolution (7.6″ × 7.5″) and filtered 25″ resolution MGCLS images in yellow and blue, respectively. The source, with a mean surface brightness of 6 μJy beam^{-1} in the full-resolution map, has a largest angular size of 5.9′, revealed in the filtered 25″ resolution image. The source appears to be 1.5 Mpc west of the MCXC J0631.3−5610 (z = 0.054) cluster centre, when comparing to an X-ray image of the region shown in Fig. 13. The total 1.28 GHz flux density of the radio source is 2.8 ± 0.2 mJy, measured from the filtered 25″ resolution image. At the cluster redshift and assuming a conservative spectral index of −1.0 with a 10% uncertainty, this corresponds to a k-corrected 1.4 GHz radio power of $(1.7 \pm 0.3) \times 10^{22}$ W Hz^{-1}.

The source has no obvious optical counterpart in the DSS r-band image of the region, shown in the right inset panel of Fig. 13, and no redshift information is available for any of the WISE sources in the region. Although showing no evidence of a radio core, it is possible that this source is a distant dying radio galaxy with the available optical imaging too shallow to identify a counterpart. However, given the morphology and orientation of the source relative to the X-ray emitting gas, it is possible that it is a relic or phoenix source related to the cluster. Its physical size would be ∼370 kpc at the cluster redshift. If this is a relic source, its radio power makes it the lowest luminosity relic known, a factor of 5 below the lowest luminosity relic listed by de Gasperin et al. (2014). With the low X-ray-derived cluster mass of $M_{500} = 1.3 \times 10^{14}\,M_{\odot}$ (Lovisari & Reiprich 2019), it

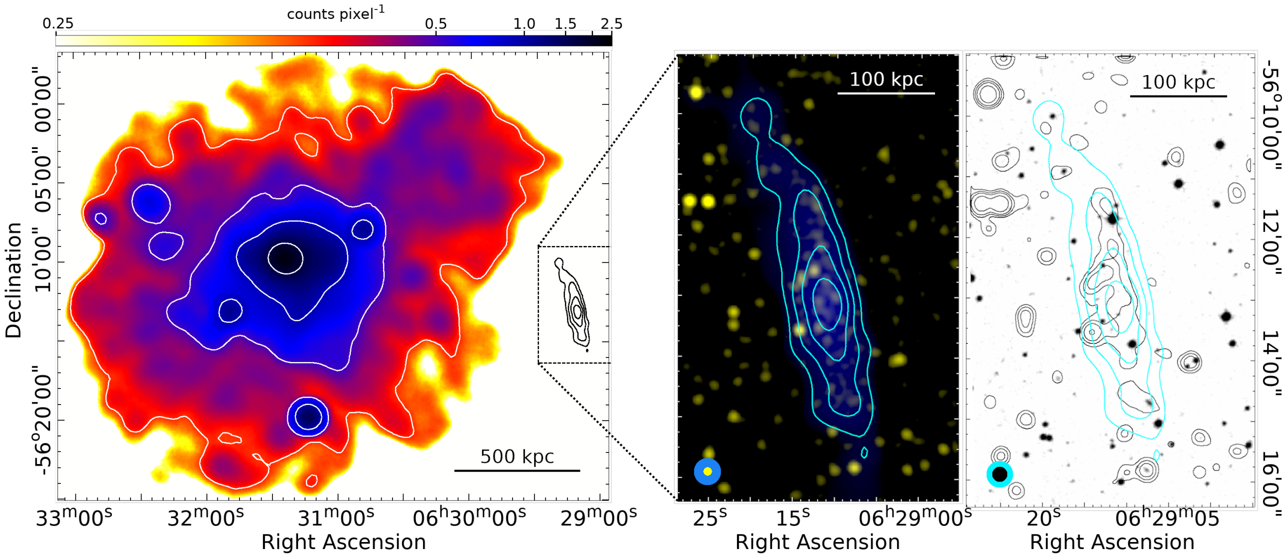

Fig. 13. Faint relic-like structure in the MCXC J0631.3−5610 (z = 0.054) cluster field. *Left*: smoothed archival *XMM-Newton* 0.2−12 keV count image of the cluster, with white contours at levels of 0.3, 0.5, 0.9, and 1.7 counts per pixel. The position of the relic-like source relative to the cluster region is indicated, with filtered 25″ resolution MGCLS contours of the radio source, to the west, in black; the radio source appears to be 1.5 Mpc from the cluster centre. *Middle*: multi-resolution MGCLS image of the radio source (yellow – 7.6″ × 7.5″ resolution; blue – filtered 25″ resolution), with cyan contours from the filtered 25″ resolution image (levels: 20, 40, 60, 80 µJy beam^{-1}). The colour scale is in square root scaling between 8−200 µJy beam^{-1} (yellow) and 5−300 µJy beam^{-1} (blue). The physical scale at the cluster redshift is shown in the upper right corner, and the synthesised MGCLS beams in the lower left corner. *Right*: DSS r-band image of the same region as the middle panel. Cyan contours are the same as in the left inset, and black contours are from the 15″ resolution MGCLS image with levels of 3, 6, 10, 20 × 1σ, where σ = 10 µJy beam^{-1}. The synthesised MGCLS beams are shown in the lower left corner. There appears to be no obvious optical counterpart for the radio source.

lies just below the extrapolation of the de Gasperin et al. (2014) luminosity-mass relation. This reinforces and extends to lower masses the problem that these radio luminosities are significantly larger than those seen in simulations (e.g. Brüggen & Vazza 2020). Observational estimates of the efficiency of shock acceleration (e.g. Botteon et al. 2020) at relics also indicate improbably high values, given our current understanding.

7. Illuminating individual radio galaxies

Among the many thousands of extended radio galaxies in the survey, we highlight a small group selected for the interesting science issues they raise. The science issues include possible missing pieces of radio galaxy physics as well as complex interactions with the external medium that go beyond the simple relative motions that created tailed radio galaxies. For each source below, we indicate if it is a member of its respective target cluster; otherwise it should be considered as a serendipitous detection.

In this section we use optical overlays from the Dark Energy Camera (DECam) Legacy Survey (DECaLS), available through the Dark Energy Legacy Survey site[12] and from the NOAO Astro Data Lab[13], and overlays from Pan-STARRS[14]. An investigation of a machine learning tool to automatically identify interesting sources is discussed in Appendix C.

7.1. Lateral edge enhancement

The laterally brightened source (LBS) shown in Fig. 14 is unique in terms of the brightening of its lateral edges, along with the presence of central jet-like features of similar length and brightness in each lobe. While some radio galaxies have bright hot spot regions at their ends (defined as Fanaroff-Riley

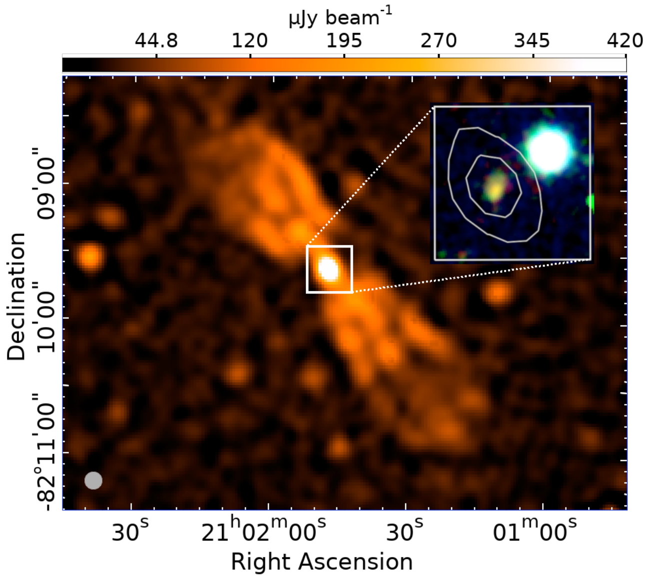

Fig. 14. Full-resolution (7.6″ × 7.4″) MGCLS Stokes-I intensity map of the LBS source, a unique double-lobed radio galaxy with lateral edge brightening. The inset is a DECam RGB colour composite (using the zir bands, respectively), with contours from the full-resolution MGCLS image showing the radio core centred at RA = 21^{h}01^{m}47.7^s, Dec = −82°09′36″ on a faint, irregularly shaped, very red object (which appears yellow-green in the zir inset). The MGCLS synthesised beam is indicated in the lower left corner.

---

[12] `https://www.legacysurvey.org`

[13] `https://datalab.noirlab.edu/ls/dataAccess.php`

[14] `https://outerspace.stsci.edu/display/PANSTARRS/Pan-STARRS1+data+archive+home+page`

type IIs, Fanaroff & Riley 1974), brightened lateral edges are not observed. Instead, radio galaxy lateral edges are observed to either cut off sharply (e.g. when pressure-confined) or to fade slowly (see e.g. Fig. 34 in Leahy & Perley 1991). The LBS was found serendipitously in the field of cluster MCXC J2104.9−8243. Here we describe some aspects of this unique source and some possibilities (none of them very attractive) for explaining the edge brightened features.

In most respects, the LBS appears normal. Its host is a faint, red, irregularly shaped object seen in the DECaLS image (see the inset in Fig. 14). No redshift is available. The NE and SW lobes have total MGCLS flux densities of 4.0 ± 0.8 and 1.9 ± 0.5 mJy, with lengths of 80″ and 100″, respectively. The length:width ratio of the lobes is ∼2:1. The source's R ratio ($S_{\rm core}/(S_{\rm total}-S_{\rm core})$, Orr & Browne 1982) is ∼14%, within the normal range, and the core has a spectral index of ∼−0.9 indicating the likely presence of small-scale optically thin jets. No reliable spectral indices could be determined for the lobes.

The lobes seem to divide abruptly into three separate lengthwise narrow features (jets and edges) at an angular distance of ∼10″ from the core. Most of the flux density appears to be in these narrow features, with little indication of more extended emission. Where the jets and enhanced edges are bright, they are each somewhat resolved transversely, with deconvolved widths of ∼5−15″. Approximately half-way to the ends, the jets and bright edges all drop by a factor of ∼2 in brightness, and the structure becomes less clear.

Jets typically fade with distance from the core, as seen here, due to expansion or other energy losses. However, the fact that the transverse edges fade at the same distance from the core as the jets do is difficult to explain in current models. We briefly considered several possible explanations for this behaviour. One possibility could be that the bright edges are due to backflow from the terminus of the jet. However, this does not appear attractive because (a) no hotspots are seen, which are expected if there is strong backflow, and (b) any edge brightening due to backflows would be brighter near the end away from the host, while we observe the opposite. Another possibility is that the bright edges are regions of strong magnetic fields, perhaps generated by shear with the external medium. However, once again, there is no reason for them to drop in brightness at the same distance from the host as the jets. A hollow cylinder could perhaps be invoked for the bright edges, similar to what is seen in some bipolar nebulae (Allen & Swings 1972), but again, the correspondence with the jet profile appears fortuitous. In short, we can provide no adequate explanation for this source's unique morphology.

7.2. Exceptionally stable bent jets

The narrow bent-tail source (NBT) shown in the top panel of Fig. 15 is unique among bent-jet sources in showing very little lateral expansion of the jets far beyond where they have bent by ∼90° from their original direction. There are many examples where no expansion may be apparent (Chibueze et al. 2021), but the resolution is insufficient to measure the widths before and after the bend. By contrast to the bent sources, straight jets can be very well-collimated, terminating in small radio and sometimes even optical hot spots subtending ≪1° as seen from the core (e.g. Roeser & Meisenheimer 1987). But bent jets such as narrow- or wide-angle tails always develop broad cocoon-like structures after the jets bend (e.g. O'Dea & Owen 1986; Rudnick & Burns 1981). As those jets bend due to their motion with respect to the surrounding medium, they tend to become unstable and are enveloped in much broader structures (O'Neill et al. 2019).

The host of the NBT is WISE 073923.89−753711.3; at a photometric redshift of $z = 0.108$ (Dálya et al. 2018) it is ∼930 kpc long, placing it in the 'giant' class. It was found serendipitously at the very large projected distance of ∼3.7 Mpc from the nearest known cluster at a similar redshift (MCXC J0738.1−7506 at $z = 0.111$). The NBT's monochromatic luminosity at 1.28 GHz is 6.4×10^{23} W Hz^{-1}, typical for bent-tail sources. Profiles across the eastern tail (top tail in Fig. 15) show that it broadens and fades until it disappears at ∼400 kpc from the host, while the western tail extends more than twice that.

In the bottom panel of Fig. 15 we compare the transverse expansion of the jets in NBT to those of NGC 1265, the prototypical head-tail/narrow-angle-tail galaxy (Miley 1973). We also include the results from a simulation of synchrotron radiation from a tailed radio galaxy with jets of internal Mach number $M = 2.5$ bent by a transverse $M = 0.9$ wind (O'Neill et al. 2019). The distances in each case are plotted as the straight line separation from the core, in units of the bending radius ($r_{\rm b}$) of the jets. For NBT we set $r_{\rm b} = 35''$, half the distance between the parallel tails; the apparent bending radius appears smaller near the host, but since the jets do not emerge exactly perpendicular to the direction of relative motion, they do not follow a simple circular path (see the appendix of O'Neill et al. 2019). The jet widths are measured as the FWHM for Gaussian fits to the jet/tail. In NGC 1265, the jets expand by a factor of 3 at 1.0 $r_{\rm b}$, while for the simulated jet, this occurs at ∼1.5 $r_{\rm b}$. By contrast, NBT reaches a factor of 3 expansion only at ∼10 $r_{\rm b}$.

It is not clear how to maintain this extraordinary collimation. In simulated jets, strong eddies form in the uniform surrounding medium, causing the jets to wobble and be partially disrupted (O'Neill et al. 2019). Pieces of jet thus transfer their momentum through the surrounding medium to the other tail, causing disruption events there. By this time, the extent of the synchrotron emitting region of each tail, mixed with the external medium, can be many times the initial jet width. The situation is even more complex if there are flow inhomogeneities in the surrounding medium.

It might appear attractive to invoke projection effects to make the bending radius appear smaller than it is in the true plane of the jets. However, to mimic the behaviour of the jets shown in Fig. 15, we need to assume foreshortening by a factor of ∼7, or an angle of ∼82° between the plane of the sky and the plane of the jets. At this angle, by the time the jets in NBT are moving parallel to one another, they would be separated by ∼1 Mpc. In comparison, the separation between the tails in narrow-angle tail sources (where the tails are parallel to each other), is typically of order 10s kpc (e.g. Gendron-Marsolais et al. 2020). Therefore, projected or not, NBT is unique in maintaining its collimation, and whether we are looking at a very special environment, or a new type of jet physics, remains a puzzle for the future.

7.3. A 300 kpc ring around interacting spirals

We discovered a ∼300 kpc diameter ring around two pairs of interacting spiral galaxies. To our knowledge, this structure is unique and not easily explained by currently known processes in such galaxies. In the full-resolution Stokes-I intensity image of the MACS J0417.5−1155 field, faint emission is seen in a ring-like structure around two compact radio sources ∼0.4° NW of and unrelated to the cluster. The ring becomes much more distinct in the filtered 25″ resolution intensity map, shown in

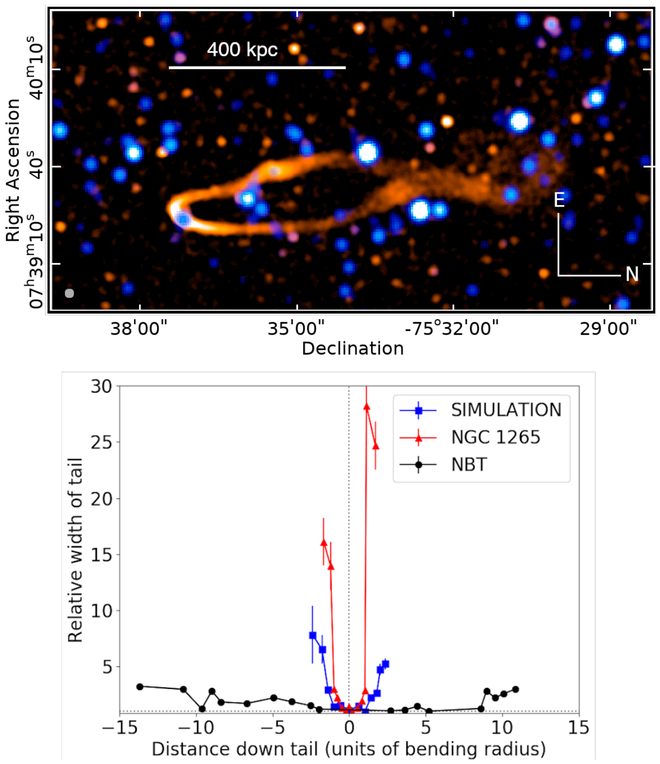

Fig. 15. Depiction of the NBT, showing that it remains well collimated long after it bends, a unique behaviour. *Top*: MGCLS Stokes-*I* full-resolution (7.5″ × 7.4″) intensity image in orange, overlaid on the WISE *W*1 image in blue. The radio brightness scale is logarithmic, saturating at 0.2 mJy beam^{-1}. The host, centred at the south end of the twin tails, is located at RA = 07^{h}39^{m}23.89^{s}, Dec = −75°37′11.3″. The physical scale at the host redshift is indicated, and the MGCLS synthesised beam is shown in lower left corner. *Bottom*: increase in jet widths, in units of the jet radius near the core, as a function of distance from the core. They show the dramatic difference between the NBT and a prototypical narrow-angle tail (NGC 1265, using the 3.7″ resolution map from Gendron-Marsolais et al. 2020) and a numerically simulated tail, from O'Neill et al. (2019).

Fig. 16. No other such rings are seen around stronger sources in this field or any other field in the MGCLS, so it is unlikely that the ring is an artefact.

Each of the bright compact radio sources near the centre overlaps a *pair* of interacting spiral galaxies, as shown in the Pan-STARRS *gri*-composite image inset in Fig. 16. The eastern radio source is centred on the brighter galaxy of its pair, WISEA J041630.96−113728.0 (also 6dFGS gJ041631.0−113728) at a redshift of 0.086 (Jones et al. 2009). The radio source is unresolved, has a flux density of 14 mJy, a spectral index of −0.76 ± 0.02, and a marginally detected ROSAT counterpart. The other galaxy in the pair, 2MASX J04163041−1137306, has a redshift of 0.087. These objects are in the foreground of the target cluster, MACS J0417.5−1155 (z = 0.44). The western radio source is also associated with the brighter member of its pair, WISEA J041628.16−113729.1, at a redshift of 0.0846, with its companion 2MASX J04162816−1137236 at a redshift of 0.083. It has a total flux density of 1.3 mJy, and a spectral index of −0.9 ± 0.05. Encircling and connecting with these compact components, the extended emission (seen in the low resolution imaging) has a total flux density of 5 ± 1 mJy and a maximum diameter of ~300 kpc, assuming it is associated with the compact sources. The luminosity of the diffuse emission and the western compact emission are each ~10^{26} W Hz^{-1}, while the eastern source's luminosity is an order of magnitude higher. All of these are orders of magnitude higher than expected from starburst activity (Condon 1992).

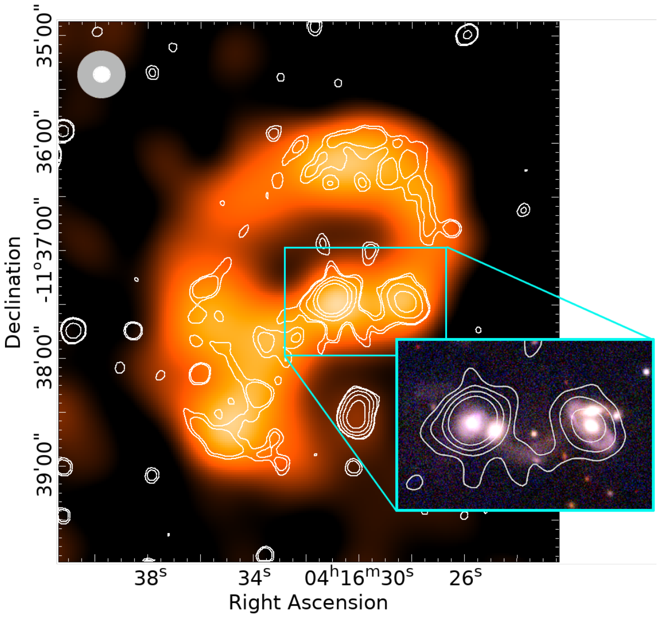

Fig. 16. Filtered 25″ resolution MGCLS Stokes-*I* intensity image of a large diffuse radio ring surrounding and connecting to an interacting pair of galaxies in the MACS J0417.5−1155 field. The brightness scale is linear and saturates at 0.2 mJy beam^{-1}. The interacting pairs are seen in the Pan-STARRS false colour *gri*-composite inset. White contours show the full-resolution (7.9″ × 7.8″) MGCLS Stokes-*I* intensity, with a 1σ local rms noise of 6 μJy beam^{-1}. The first two contours are at levels of 3.5 and 5σ, thereafter increasing by a factor of 3. The same contours, starting from 5σ, are shown in the inset. The synthesised beams are shown in the upper left corner (grey – filtered 25″ resolution, white – full resolution).

With several more galaxies, these pairs are part of the Hickson Compact Group 27 (Hickson 1982), with a diameter of 3.8′ (365 kpc), on the same scale as the radio ring. We consider first whether tidal tails could be responsible for the large ring. The tidal tails visible in the Pan-STARRS image span a smaller distance of ~73″ (115 kpc), and the lack of distortion in the galaxies suggest that the tidal interactions are still at an early stage. Tidal tails have been observed, however, to span large distances, for example 200 kpc for the HI tails of the antennas (Hibbard et al. 2001), although synchrotron emission has only been detected out to 20 kpc (Basu et al. 2017). Whether or not tidal effects could result in star formation and subsequent cosmic-ray production, along with magnetic field amplification on the scale of the ring, is an open question.

Galaxy groups, themselves, have been found to contain both extended thermal gas and relativistic plasmas, as well as large-scale H I and cold gas (e.g. O'Sullivan et al. 2018a). In some cases, thermal gas that is too diffuse to be detected in X-rays may exist on scales all the way up to 700 kpc (Freeland & Wilcots 2011), based on the distortion of radio galaxies. Nikiel-Wroczyński et al. (2019) found diffuse emission in 17 of 20 compact groups, and Nikiel-Wroczyński et al. (2013) detected diffuse radio emission extending over about 75 kpc

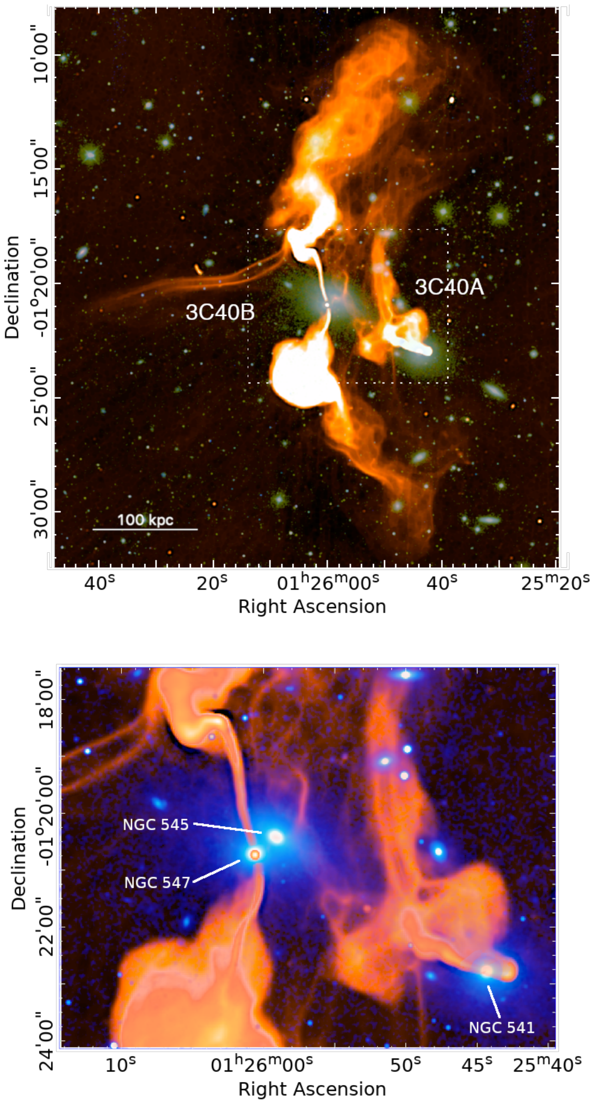

Fig. 17. Two radio galaxies in Abell 194, 3C40A, and 3C40B, with unusual filamentary appendages. *Top*: full-resolution ($7.7'' \times 7.5''$) MGCLS Stokes-I intensity image (orange), overlaid on an Sloan Digital Sky Survey (SDSS) *gri* colour composite of the region (Alam et al. 2015). The radio brightness is logarithmic, saturating at 2 mJy beam^{-1}. The physical scale at the cluster redshift of $z = 0.018$ is indicated in the lower left corner. *Bottom*: zoomed-in view of the boxed region from the top panel, with the full-resolution MGCLS image in orange on a non-monotonic scale and the SDSS r-band image in blue. The optical galaxies near the radio cores are labelled.

in Stephan's Quintet. Group-related emission has not yet been found on the physical scale or with the luminosity, or structure, shown here. The elliptical ring of emission here is brightest on its outer edges, similar to what is seen from shocks on much larger (megaparsec) scales generated when clusters of galaxies collide (peripheral radio relics). As an alternative to a shock origin, flybys of other group galaxies could light up the remnants of previous AGN activity (e.g. O'Sullivan et al. 2018b). Determining whether shocks, AGN emission, tidal tails, or some other mechanism is responsible for this curious ring-structure in J0416−1137 will depend on deeper X-ray observations and radio spectral information.

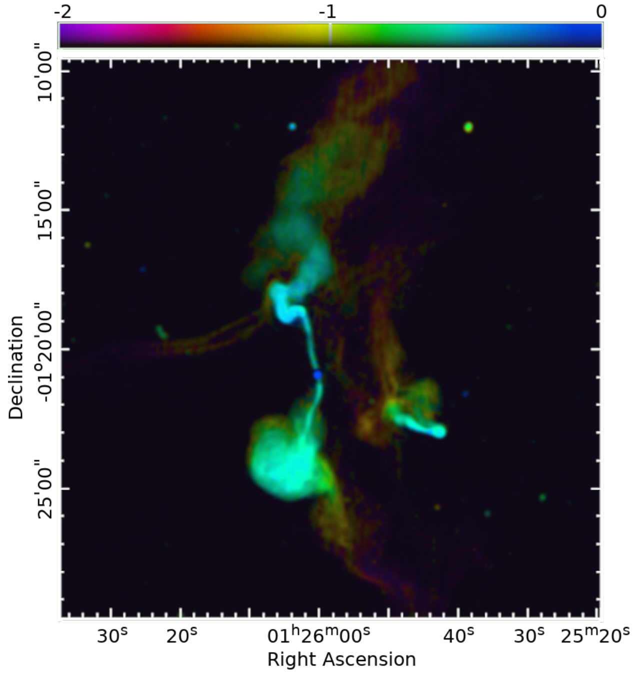

Fig. 18. Log intensity-coded MGCLS spectral index map of the 3C40A and 3C40B radio sources in Abell 194, at full resolution ($7.7'' \times 7.5''$). Colours indicate the spectral index, and the brightness indicates the Stokes-I intensity. The colour bar indicates the spectral indices, with the upper (lower) part of the colour bar corresponding to the brighter (fainter) regions. The brightness is on a linear scale and saturates at 8 mJy beam^{-1}.

7.4. The interaction of ICM magnetic filaments and radio tails

With MeerKAT's exceptional combination of sensitivity and resolution, filamentary synchrotron structures are now being discovered in the neighbourhood of radio galaxies (Ramatsoku et al. 2020; Condon et al. 2021a). Here, we present the first example where a direct interaction between a filament and the jet flow from a radio galaxy may been seen. The full-resolution MGCLS image of the Abell 194 $z = 0.018$ cluster field is shown in Fig. 17. The newly revealed filamentary structures associated with the cluster radio galaxies 3C40A and 3C40B at the centre of Abell 194 cannot be explained with any current radio galaxy models. Such very large-scale features are not seen in numerical simulations of radio galaxies, nor were such features predicted. These sources were studied at lower resolution at multiple frequencies by Sakelliou et al. (2008) who first noted unusual extensions around the radio galaxies.

The most spectacular filaments are the parallel curved pair, each $\sim$100″ (37 kpc) wide and extending 8.9′ ($\sim$200 kpc) to the east from the northern lobe of NGC 547 (3C40B). The spectral index map in Fig. 18 shows that the filamentary structures have steep spectra, similar to the faintest portions of the radio galaxy lobes. Where they appear to emerge from the northern jet, the filaments curve due SE, counter to the northern jet flow.

The second radio galaxy, 3C40A, is associated with NGC 541. At the higher MGCLS resolution, we can clearly see that the 165 kpc plumes observed by Sakelliou et al. (2008) are dominated by twin $\sim$15″ (5.5 kpc) wide filamentary structures. In addition, there is a rich network of filaments connecting to and